

# Content-decoupled Contrastive Learning-based Implicit Degradation Modeling for Blind Image Super-Resolution

Jiang Yuan, Ji Ma, Bo Wang, Weiming Hu

**Abstract**—Implicit degradation modeling-based blind super-resolution (SR) has attracted more increasing attention in the community due to its excellent generalization to complex degradation scenarios and wide application range. How to extract more discriminative degradation representations and fully adapt them to specific image features is the key to this task. In this paper, we propose a new Content-decoupled Contrastive Learning-based blind image super-resolution (CdCL) framework following the typical blind SR pipeline. This framework introduces negative-free contrastive learning technique for the first time to model the implicit degradation representation, in which a new cyclic shift sampling strategy is designed to ensure decoupling between content features and degradation features from the data perspective, thereby improving the purity and discriminability of the learned implicit degradation space. In addition, to improve the efficiency and effectiveness of implicit degradation-based blind super-resolving, we design a detail-aware implicit degradation adaption module with lower complexity, which adapts degradation information to the specific LR image from both channel and spatial perspectives. Extensive experiments on synthetic and real data prove that the proposed CdCL comprehensively improves the quantitative and qualitative results of contrastive learning-based implicit blind SR paradigm, and achieves SOTA PSNR in this field. Even if the number of parameters is halved, our method still achieves very competitive results.

**Index Terms**—Blind SR, Implicit degradation learning, Negative-free contrastive learning, Degradation adaption.

## I. INTRODUCTION

Image super-resolution (SR) is a classic low-level vision task that aims to recover a low-resolution (LR) image into its high-resolution (HR) counterpart, which has been widely used in remote sensing, video surveillance, and medical imaging, etc. In previous studies, most SR methods [1]–[8] assume that the degradation process of the image is known and fixed (e.g., bicubic downsampling), which is called the Non-Blind SR. Although somewhat successful, Non-Blind SR methods do not fit into real-world scenarios, where the image degradation is usually complex and unknown. Once the degradation assumptions of the SR methods do not align with the actual degradation, the performance will be significantly reduced [9].

This work was supported by the Beijing Natural Science Foundation(No.4234086); the Natural Science Foundation of China(No. 62192782). The work was completed during the internship in the Institute of Automation, Chinese Academy of Sciences (CASIA).

Jiang Yuan and Ji Ma are with the School of Control and Computer Engineering, North China Electric Power University, Beijing 102206, China. E-mail: yuanj@ncepu.edu.cn; maji@ncepu.edu.cn. (The two authors contribute equally to this work)

Bo Wang is with the State Key Laboratory of Multimodal Artificial Intelligence Systems, CASIA, Beijing 100190, China. E-mail: wangbo@ia.ac.cn. (Corresponding author)

Weiming Hu is with State Key Laboratory of Multimodal Artificial Intelligence Systems, CASIA, Beijing 100190, China; School of Artificial Intelligence, University of Chinese Academy of Sciences, Beijing 100049, China; School of Information Science and Technology, ShanghaiTech University, Shanghai, 201210, China. Email: wmhu@nlpr.ia.ac.cn.

Therefore, how to realize high-quality image super-resolution with unknown degradation, called Blind SR, has gradually become an emerging research topic [9]–[13].

The key to Blind SR is to effectively estimate the degradation information in LR images. Early Blind SR methods adopt an explicit degradation estimation strategy, which trains a degradation estimator to compute explicit degradation parameters from the LR image, e.g., the specific blur kernel or the noise level, as a guidance for the SR network. However, the application scope of explicit estimation-based blind SR is still limited. The unavoidable noise interference and the complex degradation combinations in real scenarios make it difficult to construct an accurate mathematical model of the degradation process, resulting in the method based on explicit estimation can only deal with some simple, low-order degradation problems. In addition, accurate numerical estimation often requires more parameters and iterations [9], making these methods time-consuming. To solve above problems, the blind SR community is gradually converting to the implicit degradation estimation strategy, which is the focus of this paper. The implicit strategy considers the degradation process to be fuzzy, so it models the degradation process as an indirect representation in the latent space. This latent representation is in line with the human fuzzy way of thinking [14], and can model the degradation process more comprehensively, which makes the estimator have stronger generalization and better robustness. At the same time, implicit degradation estimation strategy does not require extensive iterative optimization, thus significantly reducing computational costs.

The mainstream implicit estimation-based approaches use contrastive learning frameworks to model implicit representations of different degradation types, e.g., DASR [11], IDMBSR [15]. They assume that the degradations contained in different patches within the same image are consistent, while the degradation is different between patches in different images. Then, the implicit form of degradation representation is learned by pulling the positive samples closer together and pushing the negative samples farther apart. These methods initially explore the computational flow of implicit degradation estimation based on contrastive learning. However, due to the lack of systematic constraints, the implicit degradation representation learning is difficult to converge along the task-related direction and is easy to be interfered by content features such as background and appearance, resulting in the lack of sufficient discrimination of the extracted degradation features, which in turn affects the performance of image super-resolution.

To explain the problem intuitively, we reproduce the classical contrastive learning-based DASR [11] on DIV2K valset [16]. Images are first degraded using 4 different blur kernels (with kernel widths of 0.2, 1.0, 1.8, 2.6). Then patches

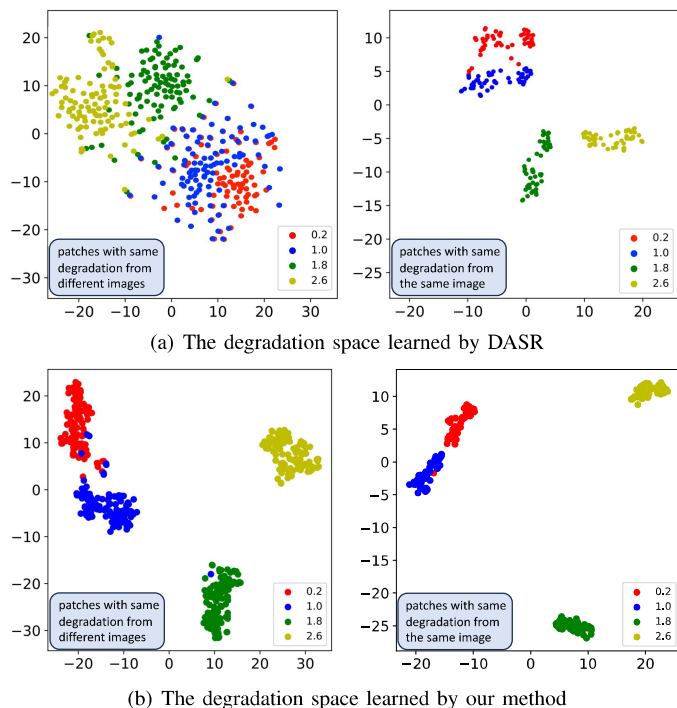


Fig. 1. The t-SNE [17] plots of degradation representation distributions with 4 different kernel widths on the DIV2K [16] val-set.

are sampled from degraded images and their degradation representations are extracted by DASR. Finally, we visualize the distribution of degradation representations by t-SNE [17]. As is shown in Fig. 1(a), for degradation space learned by DASR, if the patches with the same degradation come from different images (Fig. 1(a) left), the data distribution of each degradation is dispersed and lack discriminability between different degradations. But if the patches with the same degradation come from the same image (Fig. 1(a) right), the aggregation degree of representations for different degradations is significantly improved. This shows that the degradation space is seriously affected by content-related features.

To comprehensively improve the quality of implicit degradation modeling and SR performance under contrastive learning-based paradigm, we propose a new Content-decoupled Contrastive Learning-based image blind super-resolution (CdCL) framework (Fig. 3), which focuses on improving the implicit degradation modeling and implicit degradation adapting. In the stage of degradation modeling, by optimizing the sampling strategy, we introduce the negative-free contrastive learning method for the first time to train the implicit degradation estimator, called Content-decoupled Implicit Degradation Modeling (CdIDM). The architecture is shown in Fig. 2. The CdIDM can decouple content and degradation features, thus improving the purity and discriminability of the learned degradation representations. Specifically, instead of constructing positive pairs based on different transformations of the same image, we design a cyclic shift sampling strategy, in which patches with the same degradation from different images are sampled to construct positive pairs, thus avoiding the positive-pairing between patches with similar content, and data augmentation is achieved by continuously pairing these patches in a cyclic manner. Then, we use divide-combine operation during embedding to increase the number of positive samples of the same

degradation, thus further expanding the data diversity of each degradation category in the training stage. As shown in Fig. 1(b), regardless of the settings, the degradation space learned by our method achieves better intra-class high aggregation and inter-class high discrimination, proving that our method can learn a more discriminative feature space, where the sample clustering mainly relies on degradation information.

After obtaining high-quality degradation representations, how to effectively incorporate them into LR image features to guide the super-resolving process is also very critical, commonly known as degradation adaption. To this end, we design a more lightweight Detail-aware Implicit Degradation Adaption Module (DaIDAM) to more effectively and efficiently adapt the implicit degradation representation into the specific LR image features from both channel and spatial perspectives. The overall blind SR network architecture is shown in Fig. 3. DaIDAM consists of a large number of detail-aware degradation adaption unit (DaDAU) as basic components in series. Specifically, as shown in Fig. 4, the degradation adaption group (DAG) is first constructed by stacking a series of DaDAUs and convolution blocks, and then the DaIDAM is formed by stacking a series of DAGs and convolution blocks. Inside DaDAU, at the spatial level, instead of modulating degradation representations through continuous FC layers [11], we use two simple convolution layers to generate spatial-wise degradation coefficients, significantly reducing the number of parameters and computation. Meanwhile, when generating the channel-wise degradation coefficients, we incorporate the current LR image characteristics to adjust the intensity of the degradation coefficient of each channel. The joint learning of LR image features and channel degradation representations helps to enhance the expression of degradation information from the channel perspective, thus improving the adaption effect between them. Continuous adaption in DaIDAM can fully integrate degradation representations with LR image features, thereby better guiding the super-resolution process.

This paper constructs a new contrastive learning-based blind SR framework, whose main contributions include:

- 1) We propose a Content-decoupled Implicit Degradation Modeling (CdIDM) technique, which use negative-free contrastive learning technique to train the implicit degradation estimator, and design a new cyclic shift sampling strategy to avoid the interference of content-related features during the implicit degradation modeling process from the data perspective, so as to extract more discriminative degradation representations.
- 2) We propose a Detail-aware Implicit Degradation Adaption Module (DaIDAM), gradually modulating degradation representations from channel and spatial perspectives and adapts them to specific LR image features. It can effectively improves the adaption effect, and significantly reduces model and computational complexity.
- 3) We conduct extensive experiments on several popular benchmarks. The results demonstrate that our method greatly promotes the progress of contrastive learning-based blind SR and achieves state-of-the-art PSNR in this field. Even with a small version (50% fewer parameters), we still achieve highly competitive results.

## II. RELATED WORK

### A. Non-Blind Image Super-Resolution

As a pioneering work, SRCNN [1] was the first CNN-based SR method that outperforms previous conventional SR methods with higher efficiency and better performance using only three convolutional layers. Since then, deep learning-based SR methods [4], [5], [18], [19] have been widely studied and become the dominant SR method. VDSR [20] introduced residual modules [21] on the basis of SRCNN, and proposed a very deep SR network, which significantly improves the SR effect. To further improve the performance, RCAN [2] incorporated a channel attention mechanism [22] that adjust the importance of different feature channels in the SR network. SwinIR [23] introduced the Transformer [24] into the SR network, which improved the SR effect by establishing a larger receptive field dependence than the CNN architecture. However, since the above SR methods assume that the degradation operation is a bicubic downsampling, they usually exhibit poor performance when the test degradation is inconsistent with the expected hypothesis. To this end, some methods attach a specific degradation parameter when inputting LR images into the SR network to guide the super-resolution process. For example, SRMD [8] combined the reshaped blur kernel with the LR image as input and can generated different SR results based on the provided blur kernel. UDVD [25] also used blur kernels as an additional input to SR process and employs pixel-by-pixel dynamic convolution to more efficiently deal with changing degradation within the image. However, degradation in the real-world is often unknown, so the application scenarios of these SR methods are still limited.

### B. Blind Image Super-Resolution

In order to achieve high-quality SR in the case of unknown and mixed degradation, researchers have begun to study blind SR techniques [9], [10], [13], [26], which uses a learnable degradation estimator to extract degradation information from LR images instead of manually setting the degradation parameter. The accuracy of the estimated degradation representation largely determines the final SR performance. Early blind SR methods adopt an explicit degradation estimation strategy, which trains a degradation estimator to extract precise degradation parameters. KernelGAN [26] trained an internal GAN [27] to extract the blur kernel of a specific LR image and integrated the blur kernel into LR image features to guide the SR network. IKC [9] adopts an iterative estimation method, continuously using the generated SR image to correct the degradation representation and applying it to the next iteration until satisfactory SR results are obtained. DAN [10] designed a two-branch network to predict blur kernel and SR image in parallel and alternately updated the two branches during training, thus achieving synchronous optimization of blur kernel estimation and SR image reconstruction. Despite some progress, the above explicit degradation estimation-based SR methods often require a large number of iterations to accurately calculate degradation parameters, resulting in time-consuming and difficult to handle complex degradation.

To improve the efficiency and effectiveness of blind SR, some methods try to implicitly represent the degradation

information in the latent space without requiring specific degradation information as supervision. For example, DASR [11] learned a latent representation of degradation information through the unsupervised contrastive learning technique [28], which can handle arbitrary degradation scenario with better generalization. IDMSR [15] enhanced DASR by leveraging the blur kernel width and the noise level as weakly supervised information to guide the training of the implicit degradation estimator. DAA [29] adopted an implicit degradation modeling technique based on ranking loss [30], in which the implicit degradation estimator is trained by optimizing LR image sequences with different degradation complexities. MRDA [12] employed the meta-learning technique [31] and a multi-stage training strategy to implicitly learn the degradation representation. KDSR [32] proposed an implicit degradation estimation framework based on knowledge distillation [33], in which HR images are used to assist in training the teacher network to model different degradation types, and the learned knowledge is passed on to the student network for implicit degradation estimation in the inference stage.

## III. METHOD

### A. Overview

Given an original low-resolution (LR) image, our goal is to restore the corresponding high-resolution (HR) version in the presence of unknown degradation information. The overall architecture is shown in Fig. 3, which mainly consists of four parts: **Image feature extraction module**, which adopts a simple 3x3 convolution layer, is used to extract low-level details of the image (such as texture, color, etc.); **Implicit degradation estimation module** consists of a degradation estimator and a degradation regulator. The former is a 6-layer convolutional network trained using the proposed CdIDM technique to extract the implicit degradation representation of any LR image. The latter includes a channel transformation branch and a spatial transformation branch, which are used to further generate channel-wise degradation representation and space-wise degradation representation respectively based on the output of the estimator; **Implicit degradation adaptation module** is constructed according to the proposed detail-aware implicit degradation adapting scheme, which is used to incorporate implicit degradation representations into specific LR image features from both channel and spatial perspectives through a series of DaDAUs and DAGs. **Image reconstruction module** is used to generate a content-consistent HR image based on LR image features guided by degradation information. Here we use Upscaler [7] directly. The training of our method is divided into two stages. The first stage is to pretrain the implicit degradation estimator, and the second stage is to train the whole SR network.

### B. Content-decoupled Implicit Degradation Modeling

In order to learn more pure and discriminative degradation representations, we introduce negative-free contrastive learning technique [34], [35] to train the degradation estimator. The proposed content-decouple implicit degradation modeling framework is shown in Fig. 2, which consists of a novel cyclic shift sampling strategy and an end-to-end two-branch negative-free contrastive learning network.

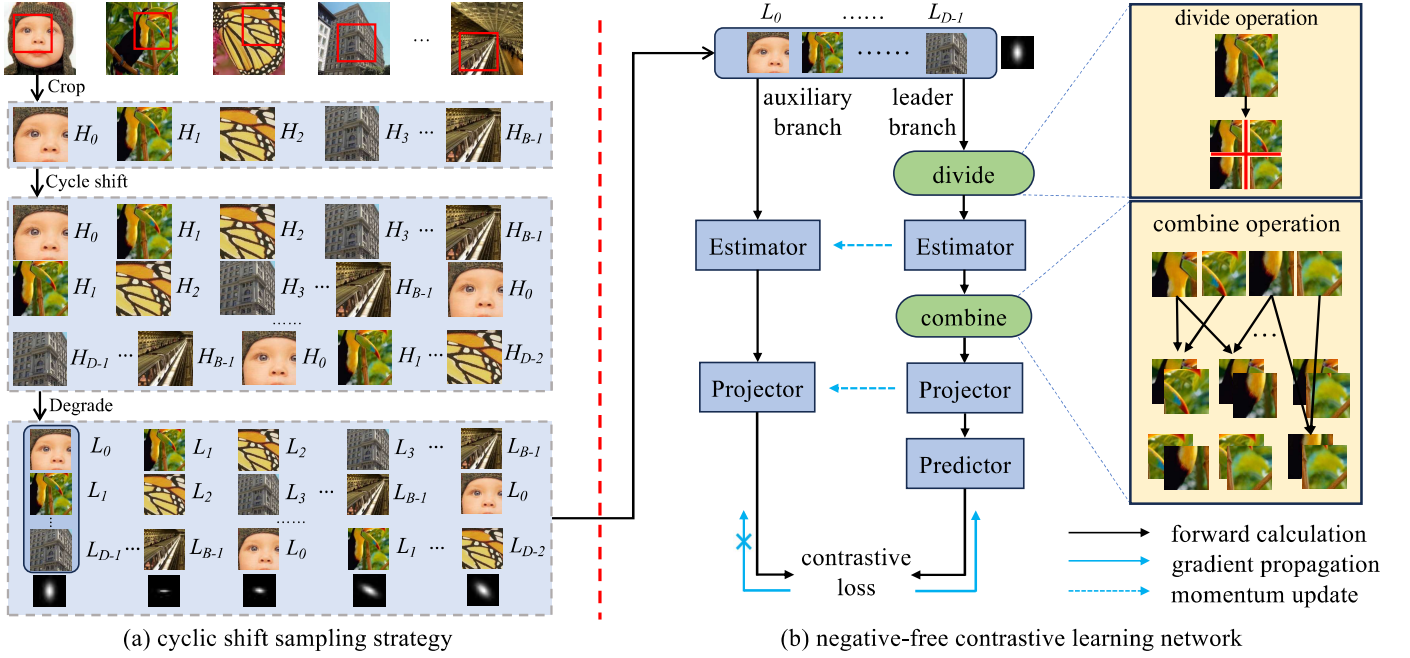


Fig. 2. The illustration of the proposed content-decouple implicit degradation modeling.

### 1) Cyclic shift sampling

A typical negative-free contrastive learning framework uses different transformations of the same sample to form positive pairs, and relies on content similarity to learn a feature space, which is exactly what implicit degradation modeling must avoid. To this end, we design a new cyclic shift sampling strategy to improve the above framework and ensure the decoupling of the learned degradation representations from the content features at the data level. Specifically, as shown in Fig. 2(a), given a set of HR images  $\mathcal{I} = \{I_0, \dots, I_{B-1}\}$ , first, we randomly sample a patch from each HR image to form a HR patch sequence  $\mathcal{S}_0 = \{S_0, \dots, S_{B-1}\}$ . Second, we cyclically shift the sequence with a step size of 1 to obtain a new sequence  $\mathcal{S}_1 = \{S_1, \dots, S_{B-1}, S_0\}$ . This operation is performed continuously  $D - 1$  times, resulting in  $D - 1$  HR patch sequences. Third, we combine the original sequence  $\mathcal{S}_0$  with all the sequences obtained by cyclic shifting to form a HR patch matrix  $\mathcal{M} = \{\mathcal{S}_0; \dots; \mathcal{S}_{D-1}\}$  with  $D$  rows and  $B$  columns. Finally, we apply a different degradation parameters to each column in  $\mathcal{M}$  to obtain the corresponding LR version of the SR patch. That is, the degradation of patches in each column is consistent, and the degradation of patches in different columns is different. In this way, we obtain  $B$  positive sample sets (each with the same degradation), which can be used to make positive pairs for subsequent contrastive learning. Meanwhile, we also get  $D \times B$  HR/LR patch pairs, which can be used for the training of the SR network.

### 2) Implicit degradation modeling

The framework for modeling degradation representations is shown in Fig. 2(b), consists of two branches: a leader branch and an auxiliary branch. The leader branch consists of an estimator, a projector, and a predictor. The estimator is a six-layer convolutional network. The projector and predictor are two-layer fully connected networks with batch-normalization [36] and GELU activation [37]. The auxiliary branch consists only of an estimator and a projector, and their structure are

the same as that in the leader branch.

During training, for the leader branch, given  $B$  positive sample sets (each consisting of  $D$  LR patches with the same degradation), each LR patch is first uniformly divided into 4 non-overlapping local blocks and sent to the estimator for encoding. Then, the encoded features are combined into 6 different pairs, and the features of each pair are averaged separately. Finally, all features are sequentially fed into the projector and predictor for continuous feature transformation. This divide-combine technique can further expand the sample diversity for each degradation category. The output of the leader branch is defined as  $\mathcal{O} \in \mathbb{R}^{B \times D \times 6 \times 256}$ , where 256 is the dimension of the implicit degradation representation. For the auxiliary branch, the LR patch is directly sent to the estimator for encoding. Then the encoded features are fed into the projector for transformation. The output of the auxiliary branch is defined as  $\mathcal{T} \in \mathbb{R}^{B \times D \times 256}$ .

The parameter update of the contrastive learning network is divided into two steps. The first step is to update the parameters of the leader branch by utilizing the contrastive loss between the outputs of the leader branch and the auxiliary branch. The loss function is defined as follows:

$$L_{contr} = \frac{1}{6D(D-1)} \sum_{i=1}^D \sum_{k=1}^6 \sum_{j=1}^D Sim(\mathcal{O}^{i,k}, \mathcal{T}^j), (i \neq j), \quad (1)$$

where the similarity function  $Sim(\cdot)$  uses InfoNCE [38]:

$$Sim(\mathcal{O}^{i,k}, \mathcal{T}^j) = \frac{1}{B} \sum_{n=1}^B -\log \frac{\exp(\mathcal{O}_n^{i,k} \cdot \mathcal{T}_n^j / \tau)}{\sum_{m=1}^B \exp(\mathcal{O}_n^{i,k} \cdot \mathcal{T}_m^j / \tau)}. \quad (2)$$

The second step is to use the momentum update technique to update the parameters of the auxiliary branch, as follows:

$$\theta_{\mathcal{T}}^{Est} \leftarrow (1-\alpha)\theta_{\mathcal{T}}^{Est} + \alpha\theta_{\mathcal{O}}^{Est}\theta_{\mathcal{T}}^{Pro} \leftarrow (1-\alpha)\theta_{\mathcal{T}}^{Pro} + \alpha\theta_{\mathcal{O}}^{Pro} \quad (3)$$

where  $\theta_{\mathcal{O}}^{Est}$  and  $\theta_{\mathcal{O}}^{Pro}$  are the parameters of the estimator and projector in the leader branch respectively,  $\theta_{\mathcal{T}}^{Est}$  and  $\theta_{\mathcal{T}}^{Pro}$  are

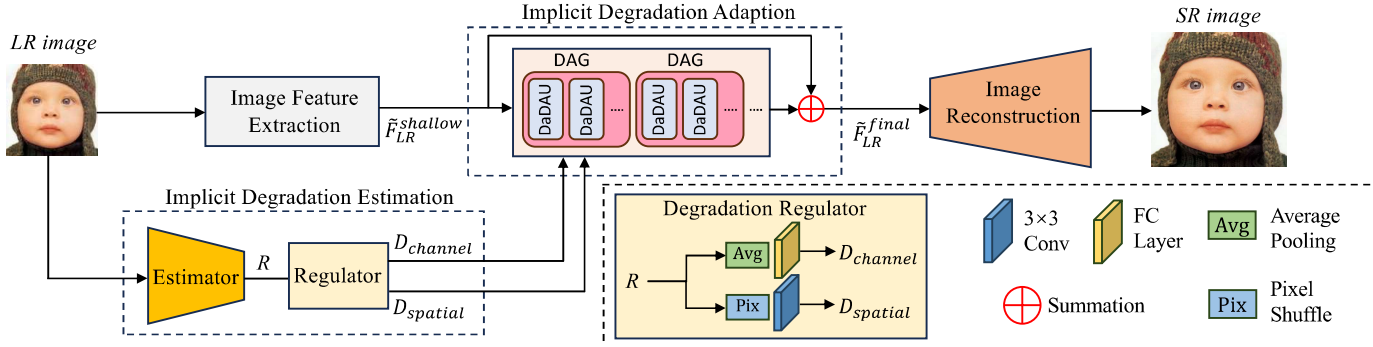


Fig. 3. The architecture of our proposed Content-decoupled Contrastive Learning-based Blind Image SR Network (CdCL).

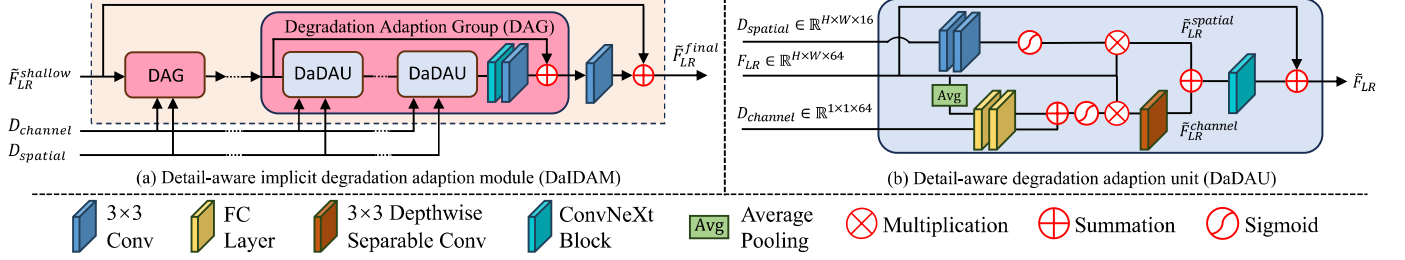


Fig. 4. The detailed structure of the DaDAU, DAG and DaIDAM.

the parameters of the estimator and projector in the auxiliary branch respectively,  $\alpha \in [0, 1]$  is the momentum coefficient. This asymmetric design helps avoid training crashes [34].

### 3) Degradation representation regulating

After training, we use only the estimator in the leader branch to extract the degradation representation of the LR image, and use the regulator to extend it from both channel and spatial perspectives. Specially, given an LR image  $I_{LR} \in \mathbb{R}^{H \times W \times 3}$  and the extracted degradation representation  $R \in \mathbb{R}^{\frac{H}{4} \times \frac{W}{4} \times 256}$ , the channel transformation branch performs global average pooling on  $R$  and sends the pooled result to a FC layer for nonlinear transformation, obtaining a channel degradation representation  $D_{channel} \in \mathbb{R}^{1 \times 1 \times 64}$ . The spatial transformation branch uses the pixel-shuffle layer [7] to upsample  $R$  to the same size as  $I_{LR}$  and sends the upsampled featuremaps into two  $3 \times 3$  convolution layers to obtain the spatial degradation representation  $D_{spatial} \in \mathbb{R}^{H \times W \times 16}$ .

### C. Detail-aware implicit degradation adapting

After obtaining degradation representations and LR image features, the adaption between them is the next key step, which determines the HR reconstruction effect. To this end, we propose a detail-aware degradation adaption unit (DaDAU) as the basic unit, and gradually construct the degradation adaption group (DAG) and the final DaIDAM, as shown in Fig. 4. Our method can significantly reduce the number of parameters while improving the network's perception of degradation details in the LR image.

#### 1) Unit level adaption

DaDAU is used for unit-level adaption, which uses a two-branch structure to modulate degradation information from both channel and spatial perspectives to fit the content details of a specific image. As shown in Fig. 4(b). In the spatial adaption branch, two  $3 \times 3$  convolution layers are first used to modulate the spatial degradation representation  $D_{spatial}$ ,

followed by a Sigmoid function for normalization. Then the modulated degradation representation is fused into the current image features  $F_{LR}$ . This process can be expressed as:

$$\tilde{F}_{LR}^{spatial} = \sigma(W_{3 \times 3}^{conv}(\tau(W_{3 \times 3}^{conv}(D_{spatial})))) \odot F_{LR} \quad (4)$$

where  $W_{3 \times 3}^{conv}$  is a  $3 \times 3$  convolution,  $\tau(\cdot)$  is the GELU activation function,  $\sigma(\cdot)$  is the Sigmoid function,  $\tilde{F}_{LR}^{spatial}$  are image features fused with spatial-wise degradation representation. In the channel adaption branch, to introduce  $F_{LR}$  in the modulation of  $D_{channel}$ , the global pooling layer is firstly used to adjust the shape of  $F_{LR}$ . Then  $D_{channel}$  and  $GAP(F_{LR})$  are fed into two FC layers at the same time, and their transformed results are added. Then a Sigmoid function is used to normalize the modulated degradation representation. Finally, the normalized result is fused into  $F_{LR}$ , followed by a  $3 \times 3$  depthwise separable convolution layer for nonlinear transformation. This process can be expressed as:

$$\tilde{F}_{LR}^{channel} = W_{3 \times 3}^{dwconv}((\sigma(W^{FC}(\tau(W^{FC}(D_{channel})))) + W^{FC}(\tau(W^{FC}(GAP(F_{LR})))))) \odot F_{LR} \quad (5)$$

where  $W_{3 \times 3}^{dwconv}$  is a  $3 \times 3$  depthwise separable convolution layer,  $W^{FC}$  is a FC layer,  $GAP(\cdot)$  is a global average pooling operation,  $\tilde{F}_{LR}^{channel}$  are image features fused with channel-wise degradation representation.

After the calculation of the two branches,  $\tilde{F}_{LR}^{spatial}$  and  $\tilde{F}_{LR}^{channel}$  are element-wise summed and fed into a ConvNeXt block [39] for further fusion. Finally,  $F_{LR}$  is fused using a residual link to recover the high-frequency detail information. This process can be expressed as:

$$\tilde{F}_{LR} = W^{Cxt}(\tilde{F}_{LR}^{spatial} + \tilde{F}_{LR}^{channel}) + F_{LR} \quad (6)$$

where  $W^{Cxt}$  is a ConvNeXt block consisting of a  $7 \times 7$  depthwise separable convolution layer and two  $1 \times 1$  convolution layers.  $\tilde{F}_{LR}$  is the degradation-adapted image features.

## 2) Group level adaption

Based on DaDAU, we construct a degradation adaption group (DAG), which consists of a series of DaDAUs, a ConvNeXt block and a 3x3 convolution layer. As shown in the red rounded rectangle in Fig. 4(a). LR image features and spatial/channel degradation representations are sequentially fed into each component for processing, and a residual link is added between the input and output of a DAG.

## 3) Module level adaption

Based on the DAG, we built the detail-aware implicit degradation adaption module (DaIDAM), as shown in Fig. 4(a), which consists of a series of DAGs and a 3x3 convolution layer in series. Similarly, we add a residual link between the input  $\tilde{F}_{LR}^{shallow} \in \mathbb{R}^{H \times W \times 64}$  and output of the DaIDAM to restore image detail features. After adaption processing, we obtain the LR image features fully fused with degradation information, defined as  $\tilde{F}_{LR}^{final} \in \mathbb{R}^{H \times W \times 64}$ .

## D. Implicit degradation-guided blind Super-resolving

### 1) Image reconstruction

After completing the adaption of implicit degradation representation and LR image features, our CdCL network use Upscaler [7] to reconstruct the corresponding HR version  $\hat{I}_{HR}$  of the input LR image. Upscaler is a learnable upsampling module composed of several convolutional layers and pixel shuffle layers, and its specific structure is determined by the scaling factor of the SR task. Given the LR image features  $\tilde{F}_{LR}^{final}$ , the reconstruction process can be expressed as:

$$\hat{I}_{HR} = \text{Upscaler}(\tilde{F}_{LR}^{final}) \quad (7)$$

### 2) Model training

During training, we use the L1 loss to update the parameters of all modules of the proposed blind SR network:

$$L_{L1} = \left\| \hat{I}_{HR} - I_{HR} \right\|_1 \quad (8)$$

where  $I_{HR}$  is the HR version of the input LR image in GT.

## IV. EXPERIMENTS

### A. Experimental Setup

#### 1) Datasets Preparation

Following [9], [11], [15], we combine 800 images from DIV2K [16] and 2650 images from Flickr2K [40] as the training dataset, and use 4 standard benchmarks (Set5 [41], Set14 [42], B100 [43] and Urban100 [44]) for quantitative and qualitative performance evaluation. Based on the above datasets, we use 3 different degradation settings to generate the LR/HR image pairs needed for training and testing. For degradation processing, we follow the classical image degradation model [45], which can be expressed as follows:

$$I_{LR} = [(I_{HR} \otimes k) \downarrow_s + n]_{JPEG} \quad (9)$$

where  $I_{HR}$  is the original HR image,  $I_{LR}$  is the degraded LR image,  $\otimes$  denotes the convolution operation,  $k$  denotes the blur kernel,  $\downarrow_s$  denotes the downsampling with the scaling factor  $s$ ,  $n$  denotes the Gaussian white noise, and  $JPEG$  denotes the JPEG compression operation. In addition, we qualitatively evaluate the generalization of the proposed method in the real-world datasets RealWorld38 [46] and RealSRSet [47].

*Degradation setting 1* contains only isotropic Gaussian blur kernels without noise and JPEG compression operation. The Gaussian kernel size is fixed to  $21 \times 21$ , the kernel width range is set to [0.2, 4.0]. The scaling factor is 3 or 4.

*Degradation setting 2* considers anisotropic Gaussian blur kernels and Gaussian white noise without JPEG compression. The anisotropic Gaussian blur kernel characterized by a Gaussian probability density function  $N(0, \Sigma)$  and the covariance matrix  $\Sigma$  is determined by two random eigenvalues  $\lambda_1, \lambda_2 \sim U(0.2, 4)$  and a random rotation angle  $\theta \sim U(0, \pi)$ . The Gaussian kernel size is fixed to  $21 \times 21$ , the Gaussian white noise range is set to [0, 25]. The scaling factor is 4.

*Degradation setting 3* covers all degradation categories, including isotropic Gaussian blur kernels, Gaussian white noise and JPEG compression. All three degradations occur with a probability of 50%. The Gaussian kernel size remains fixed at  $21 \times 21$ , the kernel width ranges from [0.1, 3.0], the noise ranges from [1, 30], the JPEG compression quality factor ranges from [40, 95]. The scaling factor is 4.

### 2) Metrics for evaluation

We use 3 metrics to assess the SR quality. Peak signal-to-noise ratio (PSNR) calculates the pixel-level similarity between SR and GT images. Structural similarity index (SSIM) [48] evaluates the low-level similarity between SR and GT images by comparing the luminance, contrast, and structure. Learned perceptual image patch similarity (LPIPS) [49] utilizes a pretrained CNN to calculate the content-level similarity. We use FLOPs as the unit of computational complexity, and all models are tested based on  $180 \times 320$  LR size.

### 3) Details for model training

For pre-processing, random flipping and random rotation are used to further augment original HR images. During entire training, the batchsize  $B$  is set to 64, the patch size is set to  $64 \times 64$ , and the number of cycle shifts  $D$  is set to 4. AdamW optimizer [50] is used for parameters updating. In the implicit degradation modeling stage, the degradation estimator is first pretrained using  $L_{contr}$  for 100 epochs, with an initial learning rate set to 1e-3 and halved at the 60th epoch. In the implicit degradation-guided blind SR network learning stage, the degradation estimator and other modules of the SR network were jointly trained for 600 epochs by summing  $L_{contr}$  and  $L_{L1}$ , with the learning rate gradually adjusted from 5e-4 to 5e-6 using the cosine annealing strategy [51]. Note that we train two versions for subsequent experiments. The small version CdCL-S includes an image feature extractor with 64 output channels and a DaIDAM with 6 DAGs. The large version CdCL-L includes an image feature extractor with 96 output channels and a DaIDAM with 8 DAGs.

## B. Comparison with Previous Methods

We conduct comparative experiments under 3 degradation settings. Comparison SR methods include SwinIR [23], KernelGAN [26], KOALANet [52], IKC [9], DAN [10], BSRGAN [47], DASR [11], IDMBSR [15], MRDA [12], and KDSR [32]. Note that except SwinIR [23], other competitors are blind SR models, among which KernelGAN [26], KOALANet [52], IKC [9] and DAN [10] are explicit degradation estimation based blind SR methods. Comparative perspectives include the qual-

TABLE I  
 ×4 SR QUANTITATIVE COMPARISON UNDER DEGRADATION SETTING 1.

Method	Param(M)	FLOPs(G)	Dataset		Set5			Set14			B100			Urban100		
			Kernel Width	1.2	2.4	3.6	1.2	2.4	3.6	1.2	2.4	3.6	1.2	2.4	3.6	
Bicubic	—	—	PSNR	27.69	25.99	24.45	25.60	24.39	23.25	25.58	24.67	23.80	22.73	21.76	20.84	
			SSIM	0.7904	0.7351	0.6774	0.6820	0.6292	0.5811	0.6461	0.5982	0.5570	0.6341	0.5791	0.5305	
SwinIR	11.9	—	PSNR	30.43	26.72	24.67	27.57	24.94	23.42	26.96	25.10	23.93	24.86	22.26	20.99	
			SSIM	0.8675	0.7660	0.6882	0.7544	0.6568	0.5896	0.7100	0.6224	0.5641	0.7468	0.6129	0.5401	
KernelGAN	0.2	—	PSNR	\	\	\	\	\	\	\	\	\	\	\		
			SSIM	\	\	\	\	\	\	\	\	\	\	\	\	
BSRGAN	16.7	—	PSNR	27.87	27.59	26.72	25.98	25.74	24.97	25.62	25.39	24.80	23.39	23.09	22.40	
			SSIM	0.806	0.7893	0.7579	0.6877	0.6668	0.6333	0.6474	0.6268	0.5931	0.6919	0.6636	0.6217	
KOALAnet	18.6	—	PSNR	30.19	28.63	26.19	27.70	26.70	24.92	27.21	27.23	25.98	24.88	24.35	22.86	
			SSIM	0.8688	0.8275	0.7470	0.7567	0.7208	0.6509	0.7296	0.7230	0.6552	0.7499	0.7229	0.6425	
IKC	5.3	2528.03	PSNR	31.76	30.35	30.26	28.44	28.17	26.63	27.43	27.28	26.41	25.63	25.02	24.07	
			SSIM	0.8870	0.8574	0.8584	0.7714	0.7606	0.7100	0.7240	0.7164	0.6854	0.7676	0.7427	0.7024	
DAN	4.3	1098.33	PSNR	32.22	31.96	30.94	28.65	28.54	27.68	27.65	27.58	26.95	26.20	25.96	25.08	
			SSIM	0.8959	0.8881	0.8659	0.7795	0.7724	0.7372	0.7343	0.7282	0.6950	0.7866	0.7758	0.7394	
DASR	5.8	185.66	PSNR	31.92	31.75	30.59	28.44	28.28	27.45	27.52	27.43	26.83	25.69	25.44	24.66	
			SSIM	0.8904	0.8855	0.8601	0.7731	0.7644	0.7293	0.7303	0.7203	0.6909	0.7700	0.7581	0.7222	
IDMBSR	4.2	—	PSNR	31.90	31.78	30.68	28.50	28.36	27.60	27.58	27.51	26.90	25.91	25.68	24.91	
			SSIM	0.8903	0.8860	0.8624	0.7770	0.7706	0.7364	0.7334	0.7278	0.6958	0.7780	0.7680	0.7330	
MRDA	5.8	172.13	PSNR	32.36	32.11	30.89	28.67	28.57	27.62	27.67	27.58	26.91	26.26	26.02	25.08	
			SSIM	0.8958	0.8900	0.8644	0.7804	0.7738	0.7344	0.7359	0.7301	0.6954	0.7889	0.7783	0.7380	
KDSR	5.8	191.42	PSNR	32.34	32.13	31.02	28.66	28.55	27.81	27.67	27.59	26.97	26.29	26.05	25.20	
			SSIM	0.8964	0.8915	0.8687	0.7865	0.7801	0.7467	0.7380	0.7320	0.6992	0.7899	0.7798	0.7455	
CdCL-S	2.9	91.68	PSNR	32.48	32.23	31.04	28.79	28.64	27.73	27.73	27.63	27.00	26.36	26.06	25.20	
			SSIM	0.8972	0.8917	0.8682	0.7835	0.7763	0.7408	0.7381	0.7316	0.6984	0.7943	0.7824	0.7460	
CdCL-L	5.9	201.68	PSNR	32.52	32.25	31.12	28.84	28.71	27.85	27.79	27.70	27.05	26.58	26.28	25.37	
			SSIM	0.8983	0.8930	0.8694	0.7843	0.7774	0.7431	0.7403	0.7343	0.7010	0.7983	0.7868	0.7502	

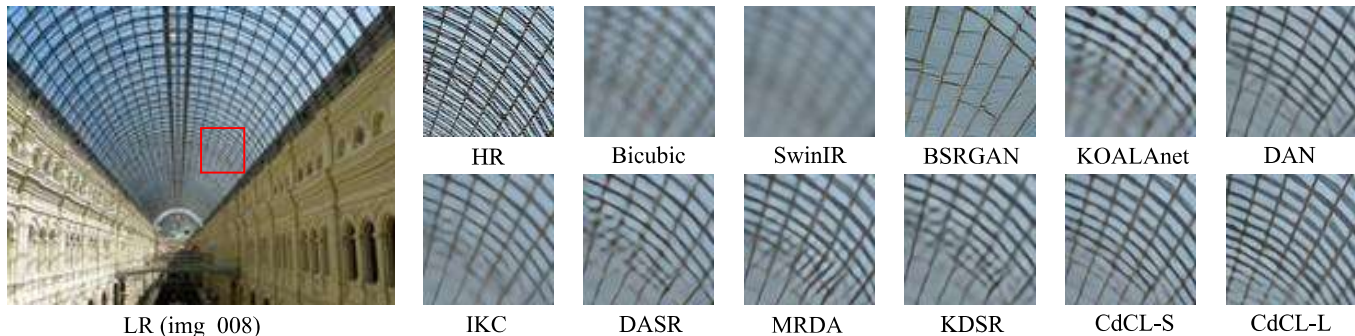


Fig. 5. The “img\_008” on Urban100, blur kernel width is 1.2, ×4 SR result.

ity of learned degradation representation, model complexity, qualitative and quantitative image SR effect.

1) Experiments in Degradation Setting 1

**Quality of implicit degradation representation.** We generate LR images from DIV2K val-set [16] under Degradation Setting 1 with scaling factor 4 and feed them to Basemodel, DASR [11], MRDA [12], KDSR [32] and CdCL to generate corresponding degradation representations. The basemodel is an blind SR network without extra implicit degradation representation learning, MRDA is meta-learning based, KDSR is knowledge distillation based, and DASR is contrastive learning based. Then we use t-SNE technique to visualize the output implicit degradation representations. Fig. 6(a) shows that it is difficult for the estimator to construct a discriminative degradation space without clear degradation learning. As can be seen from Fig. 6(b)-(e), our method achieves better degradation-based clustering, where representations of the same degradation are closer to each other and representations of different degradations are more dispersed. The comparison

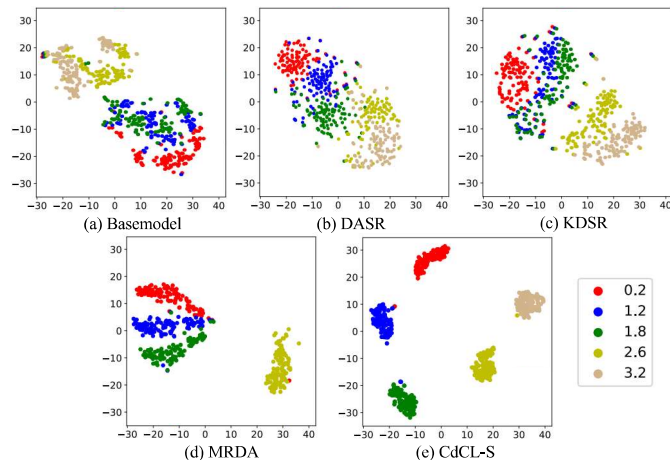


Fig. 6. The t-SNE [17] plots of degradation representation distributions with 5 different kernel widths on the DIV2K [16] val-set.

with DASR proves that excluding task-irrelevant factors helps to learn more discriminative degradation representations. The

TABLE II

$\times 3$  SR QUANTITATIVE COMPARISON UNDER DEGRADATION SETTING 1.  $\uparrow$  DENOTES THE HIGHER THE BETTER,  $\downarrow$  DENOTES THE LOWER THE BETTER.

Method	Param(M)	FLOPs(G)	Dataset	Set5			Set14			B100			Urban100		
				Width	0.8	1.6	2.4	0.8	1.6	2.4	0.8	1.6	2.4	0.8	1.6
DASR	5.7	160.37	PSNR $\uparrow$	34.08	33.94	32.50	30.03	29.88	29.21	28.90	28.82	28.23	27.42	27.12	26.33
			SSIM $\uparrow$	0.9231	0.9200	0.8983	0.8309	0.8228	0.8003	0.7940	0.7893	0.7664	0.8324	0.8235	0.7952
			LPIPS $\downarrow$	0.0820	0.0863	0.1020	0.1308	0.1360	0.1485	0.1318	0.1350	0.1456	0.1168	0.1233	0.1422
CdCL-S	2.9	67.57	PSNR $\uparrow$	34.45	34.20	33.36	30.45	30.42	29.78	29.17	29.16	28.65	28.22	28.01	27.26
			SSIM $\uparrow$	0.9265	0.9228	0.9088	0.8405	0.8370	0.8146	0.8036	0.8009	0.7771	0.8526	0.8462	0.8232
			LPIPS $\downarrow$	0.0803	0.0837	0.0958	0.1247	0.1274	0.1399	0.1270	0.1300	0.1403	0.1039	0.1085	0.1233

comparison with MRDA and KDSR proves that contrastive learning-based paradigm is still a better solution in implicit degradation modeling, and its training process is easier.

**Quantitative evaluation.** For scaling factor 4 with kernel widths  $\{1.2, 2.4, 3.6\}$ , the quantitative comparison results are shown in Table I. (1) Our method outperforms the whole explicit strategy based blind SR methods. With blur kernel widths of 1.2, 2.4, 3.6, the average PSNR/SSIM improvements of CdCL-S over DAN [10] on each dataset are 0.21dB/0.0024, 0.09dB/0.003, 0.06dB/0.003, and 0.12dB/0.007, respectively. Additionally, the proposed method reduces computational complexity by an order of magnitude compared to explicit degradation estimation based methods, thus having significant advantages in practice. (2) Compared with the existing contrastive learning-based implicit degradation estimation methods DASR [11] and IDMB SR [15], our method achieves significant improvement under multiple blur kernel widths. For example, on the Set5 [41], with blur kernel width of 2.4, our CdCL-S improves by 0.48dB and 0.45dB compared to DASR and IDMB SR, respectively, while the number of parameters is only 50% and 69% of theirs, respectively. This proves the superiority of our proposed content-decoupled implicit degradation modeling. (3) Compared with the MRDA [12] and KDSR [32] which adopts meta-learning and knowledge distillation to extract the degradation representation, with blur kernel width 1.2, our CdCL-S surpasses the MRDA by 0.12dB and the KDSR by 0.13dB (PSNR metric) on Set14, respectively. And the number of parameters and computational complexity are only about half of these methods (e.g., only 50% and 53% of MRDA, respectively). As the number of parameters increases, for PSNR, our CdCL-L achieves SOTA across all datasets with various degradation conditions. For SSIM, CdCL-L achieves SOTA on all datasets except Set14. It demonstrates that the contrastive learning-based implicit degradation modeling scheme still has a higher upper bound than the meta learning- and the knowledge distillation-based scheme. For scaling factor 3, we only compare with DASR because only it provides the quantitative results. The results are shown in Table II, with the LPIPS metric added. Similarly, our CdCL-S achieves optimal results for all datasets under different blur kernel widths with lower complexity, proving that our method has good generalization.

**Qualitative evaluation.** The super-resolved results of different models on scaling factors 4 and 3 are shown in Fig. 5 and Fig. 7, respectively. The SR images generated by our method are superior to all competitors in terms of structure and clarity. Two conclusions can be drawn: first, compared with the explicit strategy (e.g., KOALAnet, IKC, DAN), implicit

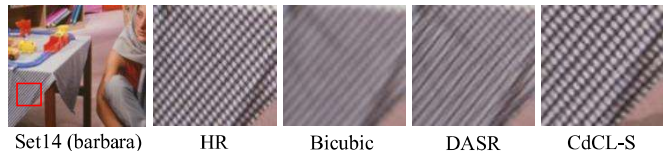


Fig. 7.  $\times 3$  SR results of “barbara” with blur kernel width 1.6.

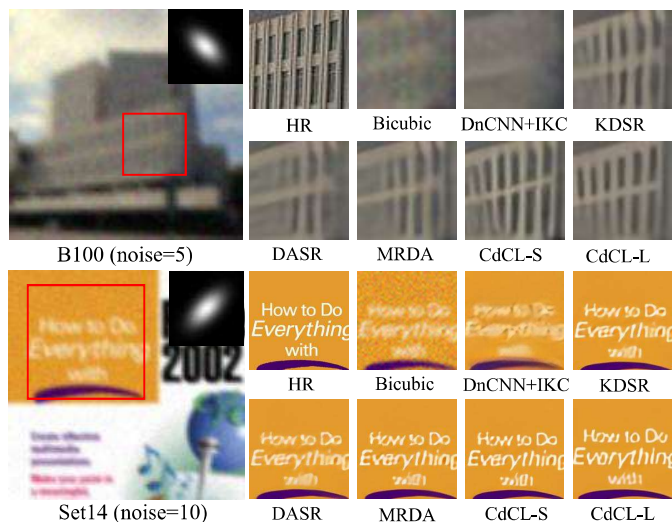


Fig. 8.  $\times 4$  SR results of the “ppt3” on Set14 and “78004” on B100 with anisotropic gaussian blur and noise.

strategy can more comprehensively model the degradation characteristics contained in images; second, compared with other implicit degradation estimation-based methods (e.g., DASR, MRDA), the degradation estimation based on content decoupling helps to more accurately restore low-level details such as local structures and textures.


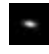
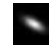
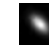
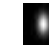





## 2) Experiments in Setting 2

**Quality of degradation representation.** In the setting 2 experiment, we generate LR images from B100 benchmark [43] under *Degradation Setting 2* with scaling factor 4 and feed them to Basemodel, DASR [11], MRDA [12], KDSR [32] and CdCL-S to generate corresponding degradation representations. Subsequently, the t-SNE plots are shown in Fig. 9. Consistent with the results of *Degradation Setting 1*, our method is still able to distinguish different degradations better than other methods and obtain the best clustering effects.

**Quantitative evaluation.** We select 9 different anisotropic blur kernels and add 2 additional noise levels (i.e., 5, 10). For RCAN [2] and IKC [9] models without denoising ability, we use DnCNN [53] to denoise LR images before SR processing for a fair comparison. Table III shows the PSNR results of our method with other competitors on the B100 benchmark



TABLE III  
 $\times 4$  SR QUANTITATIVE COMPARISON ON B100 UNDER DEGRADATION SETTING 2.

Method	Param	Noise	Blur Kernel									
												
DnCNN+RCAN	650K+15.59M	5	25.97	25.81	24.63	24.40	24.36	24.30	24.16	23.86	23.51	
		10	25.53	25.39	24.36	24.15	24.13	24.06	23.94	23.67	23.35	
DnCNN+IKC	650K+5.32M	5	26.21	26.24	25.02	24.80	24.77	24.64	24.53	24.18	23.77	
		10	25.65	25.68	24.71	24.53	24.49	24.36	24.28	24.00	23.63	
DASR	5.84M	5	26.60	26.52	25.87	25.69	25.64	25.60	25.48	25.23	24.85	
		10	26.02	25.94	25.27	25.11	25.08	25.03	24.93	24.69	24.33	
MRDA	5.84M	5	26.73	26.68	25.98	25.80	25.77	25.71	25.59	25.29	24.82	
		10	26.12	26.05	25.36	25.20	25.18	25.12	25.01	24.76	24.36	
KDSR	5.80M	5	26.73	26.70	26.02	25.87	25.83	25.76	25.65	25.37	24.94	
		10	26.11	26.05	25.38	25.24	25.21	25.15	25.05	24.81	24.46	
CdCL-S	2.87M	5	26.79	26.74	26.04	25.88	25.83	25.77	25.66	25.36	24.88	
		10	26.16	26.08	25.39	25.24	25.21	25.16	25.05	24.80	24.42	
CdCL-L	5.91M	5	26.82	26.78	26.07	25.92	25.87	25.82	25.70	25.38	24.95	
		10	26.18	26.11	25.42	25.28	25.25	25.20	25.09	24.85	24.54	

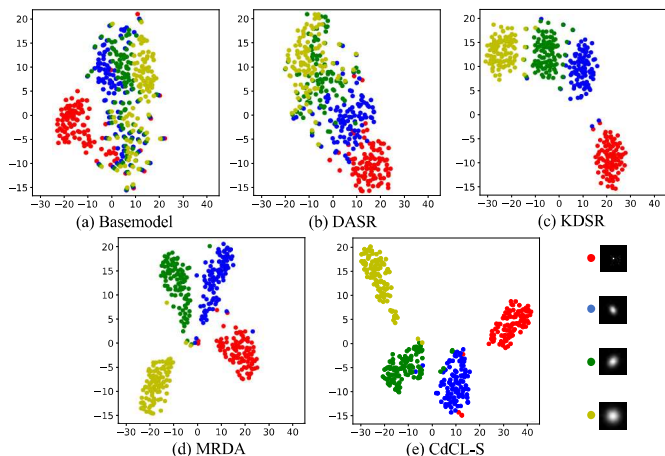


Fig. 9. The t-SNE [17] plots of degradation representation distributions with 4 different anisotropic kernels with noise level 4 on B100.

with more complex textures. It can be seen that our CdCL-L achieves SOTA performance under various noise levels and blur kernel conditions. Even if the number of parameters is halved, our CdCL-S still achieves highly competitive results. Compared with IKC [9] based on explicit degradation estimation, the average PSNR of CdCL-S is higher than IKC by over 0.83 dB, once again indicating the superiority of implicit degradation estimation. Compared with the past implicit estimation methods, our method can significantly reduce the number of parameters while improving the performance. For example, CdCL-S outperforms KDSR [32] by over 0.01 dB for the vast majority of noise levels and blur kernel conditions, but the parameters are less than half of KDSR.

**Qualitative evaluation.** Fig. 8 presents the visual results of each method under *Degradation Setting 2*. Our method can recover richer, clearer texture details even under strong noise. In contrast, the SR images generated by IKC [9] are very blurry and lack texture. The SR images generated by DASR [11] MRDA [12] and KDSR [32] have quite a lot of texture details, but they are not accurate.

### 3) Experiments in Setting 3

To further verify the generalization of our method for a wider range of degradation scenarios, we retrain DASR [11] and CdCL-S under *Degradation Setting 3*, and evaluate them on the Set14, B100, and Urban100 datasets using 8



Fig. 10. The “img\_061” on Urban100 at  $\times 4$  SR with blur kernel width 1.0, noise level 10 and JPEG compression quality factor 80.

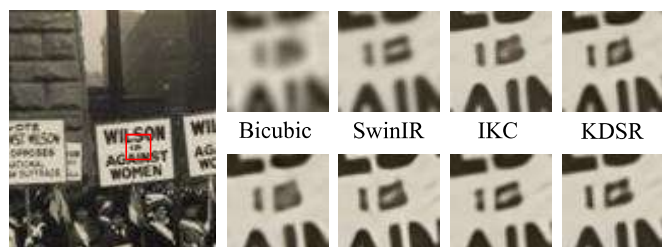


Fig. 11.  $\times 4$  SR results of the “img006” on RealWorld38 [46] under degradation setting 1.

degradation combinations described in reference [45], i.e., {bic, b2.0, n20, j60, b2.0n20, b2.0j60, n20j60, b2.0n20j60}. The comparison results are shown in Table IV. It can be seen that no matter in what kind of degradation scenarios, our method can obtain obvious performance advantages, proving that our method has better generalization. Qualitative results are displayed in Fig. 10, where the degradation parameters of LR image are blur kernel width 1.0, noise level 10, and JPEG compression quality factor 80. As can be observed from the highlighted regions, our method generates sharper texture details and smoother edges.

### 4) Experiments in Real Degradation

Finally, we validate the generalization of our method and other competitors for more challenging real degradation, where the degradation parameters are complex and unknown. Since there is no corresponding HR image, we only show the qualitative comparisons between different methods. Under the condition of *Degradation Setting 1* with scaling factor 4, the restored results of “img006” from RealWorld38 [46] by different models are shown in the Fig. 11. It can be seen that even for real images under unknown degradation, our method can recover the text portion of the LR image, which has lost a lot of high-frequency information, better than other models. In addition, we show the reconstruction of the LR image

TABLE IV  
 $\times 4$  SR QUANTITATIVE COMPARISON UNDER DEGRADATION SETTING 3.

Dataset	Method	Param(M)	Degradation Types								Average
			bic	b2.0	n20	j60	b2.0n20	b2.0j60	n20j60	b2.0n20j60	
Set14	Bicubic	—	25.00	25.34	21.77	24.29	21.91	24.51	21.46	21.73	23.25
	DASR	5.84	28.29	27.77	26.16	26.16	25.11	25.22	25.33	24.55	26.07
	CdCL-S	2.87	28.69	28.38	26.34	26.47	25.20	25.52	25.61	24.64	26.35
B100	Bicubic	—	24.63	25.40	21.56	24.06	21.90	24.65	21.22	21.72	23.14
	DASR	5.84	27.43	27.21	25.58	25.70	24.80	25.13	24.97	24.41	25.65
	CdCL-S	2.87	27.63	27.46	25.66	25.85	24.89	25.27	25.08	24.48	25.79
Urban100	Bicubic	—	21.89	22.54	20.00	21.5	20.36	22.02	19.74	20.20	21.03
	DASR	5.84	25.59	24.76	23.96	23.81	22.79	22.79	23.22	22.28	23.65
	CdCL-S	2.87	26.17	25.75	24.26	24.20	23.15	23.23	23.56	22.56	24.11

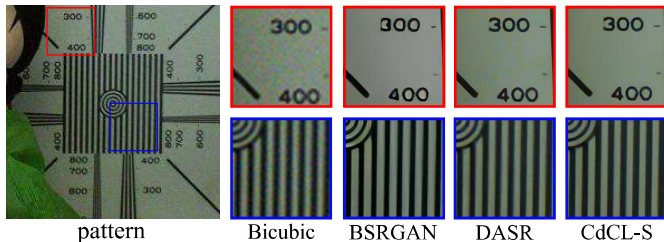


Fig. 12.  $\times 4$  SR results of the real image “*pattern*” on RealSRSet [47] under degradation setting 3.

“*pattern*” [47] by different models under the *Degradation Setting 3*, as shown in Fig. 12. In this case, although BSRGAN removes the noise better, it is not effective in recovering the digital part of the image, and it also changes the background color. In contrast, our model recovers the striped texture and digital parts of the image more clearly and accurately.

### C. Ablation Study

This section provides an in-depth analysis of our method, including the effects of the proposed Content-decoupled Implicit Degradation Modeling (CdIDM) technique and Detail-aware Implicit Degradation Adaption Module (DaIDAM), as well as the impact of different hyperparameter settings on performance. We perform full ablation experiments on all three degradation settings based on the CdCL small-version.

#### 1) Effect of the CdIDM and DaIDAM

To verify the contribution of CdIDM and DaIDAM in the contrastive learning-based blind SR network, we perform component swapping between our CdCL and DASR [11].

**For implicit degradation modeling.** We swap the degradation representation learning components between CdCL and DASR, resulting in two variants, CdCL-A and DASR-A. CdCL-A represents replacing its CdIDM with the degradation modeling framework of DASR, while keeping the rest of the network unchanged. DASR-A represents using our CdIDM to train DASR’s degradation estimator. The experimental results are shown in Table V. The SR performance of DASR-A has significantly improved, with an average PSNR 0.07dB higher than DASR on all datasets and different degradation settings. At the same time, the performance of CdCL-A has significantly decreased compared to CdCL, with an average decrease of 0.12dB in PSNR. The above results demonstrate that the proposed implicit degradation modeling technique: 1) can extract more precise degradation representations; 2) has good compatibility and can be seamlessly integrated into contrastive learning-based implicit blind SR methods.

**For implicit degradation adaption.** We swap the degradation adaption modules between CdCL and DASR, resulting in two variants, CdCL-B and DASR-B. The  $\times 4$  SR experimental results are presented in Table V. It can be observed that the use of DaIDAM can bring significant performance improvements and reduce the number of model parameters, proving that it can more effectively adapt implicit degradation representations to specific LR image features. For example, DASR-B surpasses DASR with an average PSNR 0.21dB for all datasets and degradation settings. In contrast, the average PSNR of CdCL-B is 0.18 dB lower than that of CdCL.

#### 2) Effect of different CdIDM settings

One of the design principles of CdIDM is to fully increase the sample size, which includes two key operations: cyclic shift sampling and divide-combine.

**Cyclic shift sampling operation** is used to implement data augmentation in the preprocessing stage, in which parameter  $D$  ( $D < \text{batchsize}$ ) determines the number of augmented positive samples. To verify the impact of  $D$  on SR performance, we gradually increase  $D$  from 2 to 10 and the results are displayed in Fig. 13(a). In theory, having more positive samples is more advantageous for learning discriminative degradation representations. However, in actual evaluation, we find that the model performance steadily improved as  $D$  increased from 2 to 4. But as  $D$  continues to increase, the model performance reaches saturation and even begin to gradually decline, which may be due to the redundant features caused by limited data based excessive augmenting damaging the robustness of the model to degradation distribution shifts [54].

**Divide-combine operation** is also used to augment the sample diversity of each degradation category, where the parameter  $P$  determines the scale of augmentation (dividing the input patch into  $P^2$  sub-patches on average). We set a series of increasing  $P$ -values to verify its impact on SR performance, as shown in Fig. 13(b). When  $P = 1$  (i.e., no divide-combine operation), the PSNR has a significant decrease over all degradation settings, proving the effectiveness of this operation. When  $P \geq 4$ , the PSNR gradually decreases. This is because as  $P$  increases, the size of the sub-patch seen by the estimator decreases, making it difficult to obtain sufficient information from sub-patches to learn the degradation representation. Note that the divide-combine operation is only used during training, so it does not increase the inference burden.

#### 3) Effect of different DaIDAM settings

The key to the effectiveness of DaIDAM lies in the continuous adaption between implicit degradation representation

TABLE V  
EFFECT OF THE CdIDM AND DAIDAM ON PSNR PERFORMANCE OF CdCL FOR ALL DEGRADATION SETTINGS.

Setting1										
		Set14			B100			Urban100		
	Param(M)	1.2	2.4	3.6	1.2	2.4	3.6	1.2	2.4	3.6
DASR	5.84	28.44	28.28	27.45	27.52	27.43	26.83	25.69	25.44	24.66
CdCL	2.87	28.79	28.64	27.73	27.73	27.63	27.00	26.36	26.06	25.20
DASR-A	5.84	28.53	28.30	27.47	27.60	27.49	26.89	25.78	25.54	24.75
CdCL-A	2.87	28.64	28.50	27.63	27.65	27.58	26.95	25.81	25.86	24.99
DASR-B	4.09	28.64	28.46	27.49	27.62	27.55	26.93	26.04	25.78	24.87
CdCL-B	4.39	28.57	28.48	27.54	27.61	27.56	26.95	25.9	25.63	25.03

Setting2 (Set14, noise=5)										
Param(M)										
DASR	5.84	27.25	27.18	26.37	26.16	26.09	25.96	25.85	25.52	25.04
CdCL	2.87	27.68	27.60	26.66	26.45	26.41	26.35	26.23	25.77	25.13
DASR-A	5.84	27.32	27.39	26.40	26.23	26.13	26.02	25.93	25.59	25.07
CdCL-A	2.87	27.51	27.45	26.58	26.40	26.34	26.20	26.08	25.76	25.11
DASR-B	4.09	27.44	27.36	26.49	26.32	26.24	26.12	26.02	25.67	25.09
CdCL-B	4.39	27.45	27.38	26.32	26.15	26.13	25.90	25.92	25.58	25.04

Setting3 (Urban100)										
Param(M)	bic	b2.0	n20	j60	b2.0n20	b2.0j60	n20j60	b2.0n20j60	Average	
DASR	5.84	25.59	24.76	23.96	23.81	22.79	22.79	23.22	22.28	23.65
CdCL	2.87	26.17	25.75	24.26	24.20	23.15	23.23	23.56	22.56	24.11
DASR-A	5.84	25.56	25.17	23.96	23.90	22.81	22.84	23.24	22.26	23.72
CdCL-A	2.87	25.98	25.71	24.15	23.98	23.11	23.20	23.45	22.31	23.99
DASR-B	4.09	25.78	25.50	24.15	24.08	23.05	23.20	23.43	22.50	23.96
CdCL-B	4.39	26.13	25.59	24.23	24.16	23.07	23.05	23.52	22.47	24.03

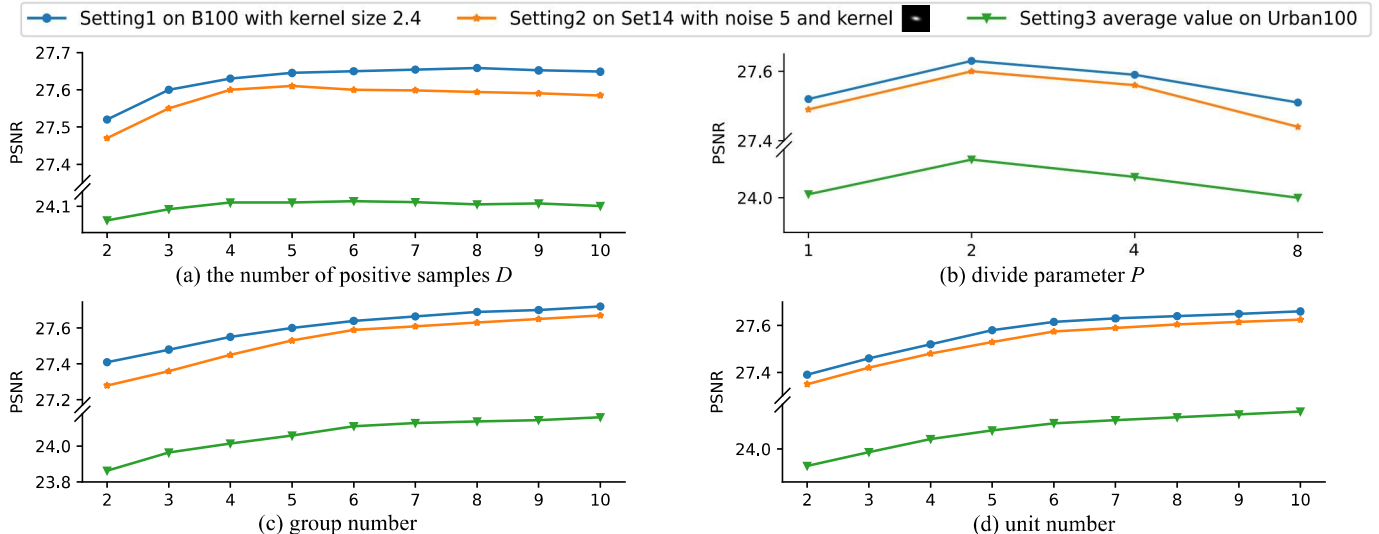


Fig. 13. The ablation study of different hyperparameters. a) Effect of the number of positive samples  $D$  in cycle shift sampling. b) Effect of the divide parameter  $P$  in CdCLIDR. c) Effect of the number of DAGs in DaIDAM. d) Effect of the number of DaDAUs in DAGs.


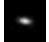

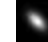





and LR image features, which involves two hyperparameter settings: the number of DaDAUs in the DAG and the number of DAGs in the DaIDAM. Specifically, we first fix the number of DaDAUs contained in each DAG to be 6, and gradually increase the number of DAGs in the DaIDAM from 2 to 10. Subsequently, we fix the number of DAGs in the DaIDAM to be 6, and gradually increase the number of DaDAUs in each DAG from 2 to 10. As can be seen in Fig. 13(c), (d), as the number of DAGs or DaDAUs increases, the SR performance steadily improves for different degradation settings, proving

the importance of continuous adaption. But as the number grows from 6 to 10, the performance improvement gradually slows down and the training time becomes longer accordingly. To balance the model complexity and performance, we choose the number of DAGs in the DaIDAM and the number of DaDAUs in the DAG to be 6 and 6, respectively.

#### 4) Effect of different DaDAU structure on SR performance

DaDAU consists of two branches that modulate degradation representations from channel and spatial perspectives and fuse them with LR image features. Following the Degradation

TABLE VI  
EFFECT OF DIFFERENT DADAU STRUCTURE ON PSNR PERFORMANCE OF CdCL FOR ALL DEGRADATION SETTINGS.

Setting1									
	Set14			B100			Urban100		
	1.2	2.4	3.6	1.2	2.4	3.6	1.2	2.4	3.6
DASR	28.44	28.28	27.45	27.52	27.43	26.83	25.69	25.44	24.66
CdCL+S	28.65	28.42	27.61	27.66	27.56	26.91	26.06	25.75	24.92
CdCL+C	28.64	28.46	27.60	27.63	27.54	26.92	26.09	25.81	25.00
CdCL+C <sub>ns</sub>	28.69	28.55	27.70	27.66	27.57	26.96	26.18	25.89	25.10
CdCL+C <sub>s</sub>	28.79	28.64	27.73	27.73	27.63	27.00	26.36	26.06	25.20
Setting2 (Set14, noise=5)									
									
DASR	27.25	27.18	26.37	26.16	26.09	25.96	25.85	25.52	25.04
CdCL+S	27.45	27.38	26.51	26.34	26.31	26.21	26.08	25.73	25.07
CdCL+C	27.52	27.43	26.52	26.31	26.21	26.10	25.91	25.47	24.70
CdCL+C <sub>ns</sub>	27.54	27.44	26.54	26.35	26.33	26.19	26.03	25.65	25.12
CdCL+C <sub>s</sub>	27.68	27.60	26.66	26.45	26.41	26.35	26.23	25.77	25.13
Setting3 (Urban100)									
	bic	b2.0	n20	j60	b2.0n20	b2.0j60	n20j60	b2.0n20j60	Average
DASR	25.59	24.76	23.96	23.81	22.79	22.79	23.22	22.28	23.65
CdCL+S	25.93	25.54	24.12	24.03	22.98	23.14	23.21	22.38	23.92
CdCL+C	26.08	25.75	24.21	24.08	23.10	23.15	23.31	22.40	24.01
CdCL+C <sub>ns</sub>	26.12	25.81	24.22	24.12	23.13	23.21	23.42	22.43	24.06
CdCL+C <sub>s</sub>	26.17	25.75	24.26	24.20	23.15	23.23	23.56	22.56	24.11

Setting 1 with scaling factor 4, we built 4 models according to Sec. III, namely CdCL+S, CdCL+C, CdCL+C<sub>s</sub> and CdCL+C<sub>ns</sub>. Among them, CdCL+S means that only the spatial adaption branch is added in DaDAU. CdCL+C means that only the channel adaption branch is added in DaDAU. CdCL+C<sub>s</sub> means that in the channel adaption branch, the two FC layers are shared between channel degradation representation  $D_{channel}$  and pooled LR image features  $GAP(F_{LR})$ . CdCL+C<sub>ns</sub> means that the two FC layers of the channel adaption branch are not shared between  $D_{channel}$  and  $GAP(F_{LR})$ . Table. VI shows the comparisons. It can be seen that even if only the spatial branch or the channel branch are used, the performance of our method is significantly better than DASR, which proves the superiority of the proposed adaption branches. In addition, the FC layers sharing mechanism in the channel adaption branch achieves better results, which we believe is due to the fact that joint learning of LR image features and channel degradation representations help to enhance the expression intensity of degradation details from the channel perspective, thereby improving the adaption effect.

## V. CONCLUSION

This paper focuses on the blind image SR task, and propose a new Content-decoupled Contrastive Learning-based blind image super-resolution (CdCL) framework, which includes two key innovations: Content-decoupled Implicit Degradation Modeling (CdIDM) technique and Detail-aware Implicit Degradation Adaption Module (DaIDAM). The former introduces the negative-free contrast learning framework to model implicit degradation and proposes a cyclic shift sampling strategy to ensure that degradation representation learning is not interfered by task-independent information at the data level, thereby improving the discriminability of the learned degradation space. The latter gradually modulates degradation

representations from channel and spatial perspectives and adapts them to specific LR image features, resulting in better SR performance and lower complexity. Extensive comparisons show that our method achieves highly competitive quantitative and qualitative results in the blind SR task, and ablation studies prove the effectiveness of the proposed components.

## REFERENCES

- [1] C. Dong, C. C. Loy, K. He, and X. Tang, "Image super-resolution using deep convolutional networks," *TPAMI*, vol. 38, no. 2, pp. 295–307, 2015.
- [2] Y. Zhang, K. Li, K. Li, L. Wang, B. Zhong, and Y. Fu, "Image super-resolution using very deep residual channel attention networks," in *ECCV*, 2018, pp. 286–301.
- [3] B. Lim, S. Son, H. Kim, S. Nah, and K. Mu Lee, "Enhanced deep residual networks for single image super-resolution," in *CVPRW*, 2017, pp. 136–144.
- [4] J.-N. Su, M. Gan, G.-Y. Chen, W. Guo, and C. P. Chen, "High-similarity-pass attention for single image super-resolution," *TIP*, vol. 33, pp. 610–624, 2024.
- [5] P. Xu, Q. Liu, H. Bao, R. Zhang, L. Gu, and G. Wang, "Fdsr: An interpretable frequency division stepwise process based single-image super-resolution network," *TIP*, vol. 33, pp. 1710–1725, 2024.
- [6] C. Ledig, L. Theis, F. Huszár, J. Caballero, A. Cunningham, A. Acosta, A. Aitken, A. Tejani, J. Totz, Z. Wang *et al.*, "Photo-realistic single image super-resolution using a generative adversarial network," in *CVPR*, 2017, pp. 4681–4690.
- [7] W. Shi, J. Caballero, F. Huszár, J. Totz, A. P. Aitken, R. Bishop, D. Rueckert, and Z. Wang, "Real-time single image and video super-resolution using an efficient sub-pixel convolutional neural network," in *CVPR*, 2016, pp. 1874–1883.
- [8] K. Zhang, W. Zuo, and L. Zhang, "Learning a single convolutional super-resolution network for multiple degradations," in *CVPR*, 2018, pp. 3262–3271.
- [9] J. Gu, H. Lu, W. Zuo, and C. Dong, "Blind super-resolution with iterative kernel correction," in *CVPR*, 2019, pp. 1604–1613.
- [10] Y. Huang, S. Li, L. Wang, T. Tan *et al.*, "Unfolding the alternating optimization for blind super resolution," in *NeurIPS*, vol. 33, 2020, pp. 5632–5643.
- [11] L. Wang, Y. Wang, X. Dong, Q. Xu, J. Yang, W. An, and Y. Guo, "Unsupervised degradation representation learning for blind super-resolution," in *CVPR*, 2021, pp. 10581–10590.

- [12] B. Xia, Y. Tian, Y. Zhang, Y. Hang, W. Yang, and Q. Liao, "Meta-learning based degradation representation for blind super-resolution," *TIP*, vol. 32, pp. 3383–3396, 2023.
- [13] S. Wu, C. Dong, and Y. Qiao, "Blind image restoration based on cycle-consistent network," *TMM*, vol. 25, pp. 1111–1124, 2022.
- [14] F. Deroncourt and E. Sander, "Fuzzy logic: between human reasoning and artificial intelligence," *Report, Ecole Normale Supérieure, Paris*, 2011.
- [15] Y. Zhang, L. Dong, H. Yang, L. Qing, X. He, and H. Chen, "Weakly-supervised contrastive learning-based implicit degradation modeling for blind image super-resolution," *KBS*, vol. 249, p. 108984, 2022.
- [16] E. Agustsson and R. Timofte, "Ntire 2017 challenge on single image super-resolution: Dataset and study," in *CVPRW*, July 2017, pp. 126–135.
- [17] L. Van der Maaten and G. Hinton, "Visualizing data using t-sne," *JMLR*, vol. 9, no. 11, 2008.
- [18] H. Lee, J.-S. Yoo, and S.-W. Jung, "Refqsr: Reference-based quantization for image super-resolution networks," *TIP*, vol. 33, pp. 2823–2834, 2024.
- [19] Z. Li, Z.-S. Kuang, Z.-L. Zhu, H.-P. Wang, and X.-L. Shao, "Wavelet-based texture reformation network for image super-resolution," *TIP*, vol. 31, pp. 2647–2660, 2022.
- [20] J. Kim, J. K. Lee, and K. M. Lee, "Accurate image super-resolution using very deep convolutional networks," in *CVPR*, 2016, pp. 1646–1654.
- [21] K. He, X. Zhang, S. Ren, and J. Sun, "Deep residual learning for image recognition," in *CVPR*, 2016, pp. 770–778.
- [22] J. Hu, L. Shen, and G. Sun, "Squeeze-and-excitation networks," in *CVPR*, 2018, pp. 7132–7141.
- [23] J. Liang, J. Cao, G. Sun, K. Zhang, L. Van Gool, and R. Timofte, "Swinir: Image restoration using swin transformer," in *CVPR*, 2021, pp. 1833–1844.
- [24] A. Vaswani, N. Shazeer, N. Parmar, J. Uszkoreit, L. Jones, A. N. Gomez, Ł. Kaiser, and I. Polosukhin, "Attention is all you need," *NeurIPS*, vol. 30, 2017.
- [25] Y.-S. Xu, S.-Y. R. Tseng, Y. Tseng, H.-K. Kuo, and Y.-M. Tsai, "Unified dynamic convolutional network for super-resolution with variational degradations," in *CVPR*, 2020, pp. 12496–12505.
- [26] S. Bell-Kligler, A. Shocher, and M. Irani, "Blind super-resolution kernel estimation using an internal-gan," *NeurIPS*, vol. 32, 2019.
- [27] I. Goodfellow, J. Pouget-Abadie, M. Mirza, B. Xu, D. Warde-Farley, S. Ozair, A. Courville, and Y. Bengio, "Generative adversarial networks," *Commun. ACM*, vol. 63, no. 11, p. 139–144, oct 2020.
- [28] K. He, H. Fan, Y. Wu, S. Xie, and R. Girshick, "Momentum contrast for unsupervised visual representation learning," in *CVPR*, 2020, pp. 9729–9738.
- [29] Y. Wang, J. Ming, X. Jia, J. H. Elder, and H. Lu, "Blind image super-resolution with degradation-aware adaptation," in *ACCV*, 2022, pp. 894–910.
- [30] W. Zhang, Y. Liu, C. Dong, and Y. Qiao, "Ranksrgan: Generative adversarial networks with ranker for image super-resolution," in *ICCV*, 2019, pp. 3096–3105.
- [31] C. Finn, P. Abbeel, and S. Levine, "Model-agnostic meta-learning for fast adaptation of deep networks," in *ICML*, 2017, pp. 1126–1135.
- [32] B. Xia, Y. Zhang, Y. Wang, Y. Tian, W. Yang, R. Timofte, and L. Van Gool, "Knowledge distillation based degradation estimation for blind super-resolution," in *ICLR*, 2023.
- [33] G. Hinton, O. Vinyals, and J. Dean, "Distilling the knowledge in a neural network," *arXiv preprint arXiv:1503.02531*, 2015.
- [34] J.-B. Grill, F. Strub, F. Altché, C. Tallec, P. Richemond, E. Buchatskaya, C. Doersch, B. Avila Pires, Z. Guo, M. Gheshlaghi Azar *et al.*, "Bootstrap your own latent—a new approach to self-supervised learning," *NeurIPS*, vol. 33, pp. 21271–21284, 2020.
- [35] Y. Ci, C. Lin, L. Bai, and W. Ouyang, "Fast-moco: Boost momentum-based contrastive learning with combinatorial patches," in *ECCV*. Springer, 2022, pp. 290–306.
- [36] S. Ioffe, "Batch renormalization: Towards reducing minibatch dependence in batch-normalized models," *NeurIPS*, vol. 30, 2017.
- [37] D. Hendrycks and K. Gimpel, "Gaussian error linear units (gelus)," *arXiv preprint arXiv:1606.08415*, 2016.
- [38] A. v. d. Oord, Y. Li, and O. Vinyals, "Representation learning with contrastive predictive coding," *arXiv preprint arXiv:1807.03748*, 2018.
- [39] Z. Liu, H. Mao, C.-Y. Wu, C. Feichtenhofer, T. Darrell, and S. Xie, "A convnet for the 2020s," in *CVPR*, 2022, pp. 11976–11986.
- [40] R. Timofte, E. Agustsson, L. Van Gool, M.-H. Yang, and L. Zhang, "Ntire 2017 challenge on single image super-resolution: Methods and results," in *CVPRW*, July 2017, pp. 114–125.
- [41] M. Bevilacqua, A. Roumy, C. Guillemot, and M. L. Alberi-Morel, "Low-complexity single-image super-resolution based on nonnegative neighbor embedding," in *BMVC*, 2012.
- [42] R. Zeyde, M. Elad, and M. Protter, "On single image scale-up using sparse-representations," in *Curves and Surfaces*. Springer Berlin Heidelberg, 2012, pp. 711–730.
- [43] D. Martin, C. Fowlkes, D. Tal, and J. Malik, "A database of human segmented natural images and its application to evaluating segmentation algorithms and measuring ecological statistics," in *ICCV*, vol. 2, 2001, pp. 416–423 vol.2.
- [44] J.-B. Huang, A. Singh, and N. Ahuja, "Single image super-resolution from transformed self-exemplars," in *CVPR*, 2015, pp. 5197–5206.
- [45] W. Zhang, G. Shi, Y. Liu, C. Dong, and X.-M. Wu, "A closer look at blind super-resolution: Degradation models, baselines, and performance upper bounds," in *CVPR*, 2022, pp. 527–536.
- [46] J. Liang, H. Zeng, and L. Zhang, "Efficient and degradation-adaptive network for real-world image super-resolution," in *ECCV*. Springer, 2022, pp. 574–591.
- [47] K. Zhang, J. Liang, L. Van Gool, and R. Timofte, "Designing a practical degradation model for deep blind image super-resolution," in *ICCV*, 2021, pp. 4791–4800.
- [48] Z. Wang, A. C. Bovik, H. R. Sheikh, and E. P. Simoncelli, "Image quality assessment: from error visibility to structural similarity," *TIP*, vol. 13, no. 4, pp. 600–612, 2004.
- [49] R. Zhang, P. Isola, A. A. Efros, E. Shechtman, and O. Wang, "The unreasonable effectiveness of deep features as a perceptual metric," in *CVPR*, 2018, pp. 586–595.
- [50] I. Loshchilov and F. Hutter, "Decoupled weight decay regularization," in *ICLR*, 2018.
- [51] I. Loshchilov and F. Hutter, "SGDR: stochastic gradient descent with warm restarts," in *ICLR*, 2017.
- [52] S. Y. Kim, H. Sim, and M. Kim, "Koalnet: Blind super-resolution using kernel-oriented adaptive local adjustment," in *CVPR*, 2021, pp. 10611–10620.
- [53] K. Zhang, W. Zuo, Y. Chen, D. Meng, and L. Zhang, "Beyond a gaussian denoiser: Residual learning of deep cnn for image denoising," *TIP*, vol. 26, no. 7, pp. 3142–3155, 2017.
- [54] G. Ortiz Jimenez, A. Modas, S. M. Moosavi DeZfooli, and P. Frossard, "Redundant features can hurt robustness to distributions shift," in *ICML*, 2020.